This is a repository copy of *Effect of graphene oxide on the mechanical properties and the formation of layered double hydroxides (LDHs) in alkali-activated slag cement*.

White Rose Research Online URL for this paper:
http://eprints.whiterose.ac.uk/111910/

Version: Accepted Version

Article:

Effect of graphene oxide on the mechanical properties and the formation of layered double hydroxides (LDHs) in alkali-activated slag cement

Xiao Hong Zhu[a], Xiao Juan Kang[a], Kai Yang[a, *], Chang Hui Yang[a, b*]

[a] College of Materials Science and Engineering, Chongqing University, Chongqing 400044, P.R. China

[b] Chongqing Key Laboratory of New Building Materials and Engineering, Chongqing University, Chongqing 400044, P.R. China

*Corresponding author. College of Materials Science and Engineering, Chongqing University, Chongqing, P.R. China

E-mail address: ychh@cqu.edu.cn (C. H. Yang), yang.kai@cqu.edu.cn (K. Yang).

Highlights:
(1) Graphene Oxide (GO) caused a significant reduction in fluidity and a slight decrease in compressive strength of AAS mortars.
(2) The flexural strength of hardened mortars were improved by adding GO.
(3) Layered double hydroxides (LDHs) were observed and confirmed in GO-added AAS system.

Abstract

Due to its high aspect ratio and outstanding tensile strength, graphene oxide (GO) can dramatically reduce the brittleness of cement-based materials. In this paper, GO nanosheets were successfully synthesised using the modified Hummers' method. Effects of the GO on the fluidity, mechanical properties of alkali-activated slag (AAS) mortars and the microstructure of the AAS pastes were studied. It is found that addition of the GO caused a significant reduction in fluidity and a slight decrease in the compressive strength of the hardened mortars. However, the GO improved the flexural strengths by 20% with a dosage of 0.01 wt. % after 7 days. Large-scale layered double hydroxides (LDHs) were observed using SEM, the compositions of which were identified and EDS and XRD. A possible mechanism of the formation of LDHs in the GO-AAS system is proposed. Due to the Mg^{2+}/Al^{3+} decomposed from the slag and the $Al(OH)_4^-$ formed in the high pH condition in the GO-AAS system, the reaction pathway of LDHs

can be regarded as

$$aMg^{2+} + Al(OH)_4^- + (2a-2)OH^- + xH_2O + A^- \rightleftharpoons Mg_aAl(OH)_{2+2a}A \cdot xH_2O(s)$$
,
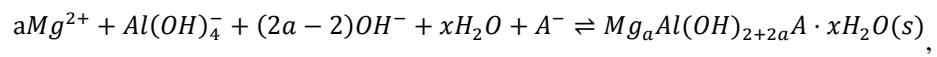
This research provides a further understanding of the effect of graphene oxide which has a potential application of GO in AASC.

1. Introduction

Alkali-activated slag cement (AAS), which can be a clinker-free binder, provides an eco-friendly alternative to conventional Portland cement [1]. The use of granulated ground blast furnace slag (GGBFS) as the precursor provides a significant lower carbon dioxide emission as well as lower energy consumption than ordinary Portland cement (OPC) [2-5]. Furthermore, AAS has high compressive strength [1, 6], resistance to chemical attacks [1, 7] and better immobilization of heavy metals [8]. However, due to the higher drying shrinkage and brittleness [8-9], an easier tendency of cracking for AAS has been reported by previous reports [2-3, 9-10]. Different fibres have been introduced to improve its toughness [11-12].

The development of nano-materials, e.g. carbon nanofibres, carbon nanotubes and graphene, has offered an opportunity to improve the toughness of cement-based materials [13]. The combination of cement with a small amount of carbon material has an admirable impact on the mechanical behaviour of OPC and other inorganic cements [13-16]. Of all of the carbon-based materials, two-dimensional (2D) graphene oxide (GO) sheets with an ultra-high dispersibility and a superior aspect ratio compared to other nano-carbon materials show a suitable performance in a cement matrix [13, 17]. Previous studies [13-14, 18] have shown that the introduction of a small amount of GO (0.05 wt. %) can increase the compressive strength by approximately 30% and the flexural strength by approximately 50%. Moreover, the unique rough surface of GO with many functional groups (-OH, -COOH and -O-) has a seeding effect on the hydration kinetics in cement. Lv et al. [19] found that use of GO nanosheets could produce bar-like and flower-like crystals in OPC that are the hydration products in the system and regarded as the reason for the improvement in mechanical properties. In addition, calcium-type cross-linking has been found in OPC due to the presence of the carboxyl and hydroxyl groups of GO [20], which can minimise

the pore size and form strong interfacial adhesion to the cement matrix. Therefore, GO bridges the two

main hydration products (CSH gel and $Ca(OH)_2$). The presence of GO in the AAS system can also form

silica-type cross-linking in geopolymeric composites to enhance the mechanical properties of

geopolymers [21]. Based on a similar type of products in AAS (C-A-S-H), the GO should have high

performances in strongly linking hydration products. Moreover, some divalent ions (Mg^{2+} and Ca^{2+})

could also enhance the influences of GO [22], as with the decomposition of GGBFS, some divalent ions

could exist in the liquid phase.

In this research, graphene oxide was synthesised using the modified Hummers' method. The fluidity,

mechanical properties and hydration products of the AAS were investigated. Experimental results show

that the incorporation of GO nanosheets improved the flexural strength of AAS significantly and had a

noticeable impact on the formation of layered double hydroxides (LHDs) in AAS. The formation

mechanism of LDHs in GO-supplemented AAS has been proposed based on this study.

2. Experimental Procedure

2.1 Preparation of graphene oxide

Graphene oxide was produced based on the modified Hummers' method. Graphite powder (2

g) and $NaNO_3$ powder (1 g) were added into a 1000-ml round-bottom flask and then concentrated

H_2SO_4 (100 ml) was slowly added into the flask in an ice bath. After 4 hours, $KMnO_4$ (6.0 g) was

slowly added and stirred into the flask for 20 minutes in an ice bath. The flask was then moved out

of the ice bath, and the sample was continuously stirred at room temperature for a further 24 hours.

Then, the resulting mixture was mixed with deionized water (200 ml) to obtain a dispersion by stirring

at 0 °C for 20 min, followed by a slow addition of H_2O_2 (10 ml) using a pipette gun to dissolve the

MnO_2 produced from the oxidation reaction between graphite and $KMnO_4$. Sodium nitrate,

concentrated sulfuric acid, potassium permanganate oxidises double bond into hydroxyl and carboxyl groups and struts piece layer. The role of the hydrogen peroxide is to restore the excess of potassium permanganate. The obtained dispersible mixture was filtered through a Buchner funnel, and then HCl aqueous solution (20 ml) was transferred to the flask using a pipette gun to react with the SO_4^{2-}. The products were then stirred with running ultrapure water for 4 days to remove some of those metal ions and residual acid. Finally, the prepared graphene oxide solution was purified by centrifugation four times, and then the solution was sucked with a vacuum suction filtration device to stop the repetition of the filtration process until the pH reached a neutral value. The obtained neutral graphene oxide particles were used in this investigation.

2.2 Preparation of AAS pastes and mortars

The starting material used in this investigation is a GGBFS from Chongqing Iron and Steel Company. The basicity coefficient ($M_0 = \frac{wCaO + wMgO}{wSiO_2 + wAl_2O_3}$) and activity coefficient ($M_a = \frac{wAl_2O_3}{wSiO_2}$) are 1.03 and 0.45, respectively. Its specific gravity and Blaine fineness are 2.95 g/cm^3 and 435 m^2/kg, respectively. A commercial sodium silicate solution, composed of 29.3% SiO_2, 12.07% Na_2O and 51.4% H_2O by mass, was used as the alkaline activator of the GGBFS. The XRD pattern (Fig. 1) of the anhydrous GGBFS shows that the main crystalline phase is akermanite ($Ca_2MgSi_2O_7$, PDF# 074-0990), and there are also minor traces of calcite ($CaCO_3$, PDF# 70-0095). The content of alkali was 5% by weight of GGBFS, and the modulus ($M_s = SiO_2/Na_2O$) of sodium silicate was changed from the initial 2.46 to the final 1.2 by using NaOH (AR). The GO content ranged from 0.01% to 0.05% by weight of the GGBFS.

The water to binder ratio of all the samples was 0.4, and the binder to sand ratio of all the mortars was 1:3. The fluidity and mechanical properties were tested with AAS mortars, while XRD and SEM-EDS analysis were carried out with AAS pastes.

2.3 Methods

2.3.1 Macroscopic properties

The fluidity was evaluated by jump table tests performed according to Chinese Standard: GB/T 2419-2005. The fresh mortar was filled into a truncated conical model with inner diameters of 70 mm (upper end) and 100 mm (bottom) with a height of 60 mm. Then, the mould was removed and the table was started vibration with a frequency of 60 r/min. After 25 seconds, the diameter of the mortar expansion was measured as the fluidity.

The mechanical properties of all the specimens were measured as per Chinese standard GB/T 17671-1999 at 3 days, 7 days and 28 days. The specimens were cured in a standard condition (Temperature = 20±1℃, relative humidity ≥ 95%).

2.3.2 Microstructural characterisation

The oxygen functional groups of the GO were identified using Fourier transform infrared (FTIR) spectrometry (Nicolet iS5, Thermo Scientific). The hydration products of AAS were recorded by powder X-ray diffraction (XRD, PIGAKV D/max 1200, Cu Kα).

Scanning electron microscopy (SEM) was performed using a TESCAN VEGA 3 LMH instrument with a 20 kV accelerating voltage [23]. The selected samples were vacuum-dried at 50℃ for 48 hours and then coated with gold. An energy dispersive spectroscopy (EDS, Oxford Instrument) detector was used to determine chemical compositions.

3. Results and Discussion

3.1 Characterisation of graphene oxide

The SEM image of the GO is shown in Fig. 2. As indicated, ultrathin and well-dispersed GO nanosheets were successfully prepared. Fig. 3 gives the XRD spectrum of the GO. A typical single strong

peak appeared at approximately 10° [24], which indicates that the oxygen functional groups have penetrated onto the surface of graphene. An average thickness of 0.328 nm (single sheet) was also calculated from the XRD pattern according to the Scherrer equation with a constant (K) equal to 0.89 [24].

The FTIR spectrum of the GO is displayed in Fig. 4. The vibrations of the characteristic oxygen functional groups can be detected through FTIR analysis [25]. The adsorption peaks of the GO in Fig. 4 are as follows: 3416.62 cm^{-1} is the vibration of hydroxyl (-OH); 1720.72 cm^{-1} is attributed to carboxyl (-COOH); the absorption peaks between 950 cm^{-1} and 1275 cm^{-1} are corresponding to the stretching of carbonyls (C-O-), which include C-OH (1200 cm^{-1} - 950 cm^{-1}), C-O-CO (1275 cm^{-1} - 1150 cm^{-1}) and C-O-C (1270 cm^{-1} - 1050 cm^{-1}); and 1201.15 cm^{-1} and 980.52 cm^{-1} are the peaks of the $-SO_3H$ groups on the surface of the GO nanosheets. These similar functional groups were also detected in other studies [17, 19, 23-24].

The above results show the characteristics of the synthetic GO nanosheets used in this research. The functional groups and the zeta potential of GO can aid in its dispersion into the alkaline solution [26-27]. Due to its special structure and surface properties, GO might be more suitable for use in the AAS system.

3.2 Fluidity and mechanical properties of AAS mortars

The fluidity of AAS mortars containing different solid dosages of GO (0.01%/0.03%/0.05% by weight of slag) is summarised in Table 2. The plain AAS mortar with a water to binder ratio of 0.4 had a fluidity of approximately 215 mm. However, with a dosage of GO of 0.05%, the fluidity of the mortars was reduced to approximately 155 mm, 27.91% lower than that of the reference AAS mortar. The results show a notable reduction trend in the fluidity of the AAS mortar with the increasing GO dosage, which is consistent with previous research on the phenomenon of nanomaterial-added cement specimens [13,

28-29]. A possible reason is that the large surface area of the hydrophilic GO could absorb more water in the system, so that there might be less free water that is related to the rheological behaviour of the mortar [13, 18].

The compressive and flexural strengths of the AAS mortars with GO at 3 days, 7 days and 28 days are also given in Table 2. It can be found that the flexural strengths of all of the GO-added specimens increased, and the optimal content was approximately 0.01 wt. %. The increase rate of the flexural strength at a dosage of 0.01 wt. % was approximately 20% after 7 days. However, this is inconsistent with the optimal content of GO in the OPC system, which is approximately 0.03% - 0.04%, as reported in previous studies [14, 19, 28]. Interestingly, the data of the compressive strengths of all the specimens with the addition of GO showed a slight decreasing tendency, except for GM-1 at 28 days, quite different from the trend for OPC [13-14, 18-19, 28]. The compressive and flexural strengths are determined by the synergetic effect of the GO itself and the microstructures that are formed in its presence [14].

3.3 Microstructural investigations

SEM images of AAS pastes with additions of different amounts of GO at 28 days are shown in Fig. 5. Without the GO, the typical rocklike hydration products mainly consist of C-(A)-S-H gel together with the remaining slag particles (lighter and angular part of Fig. 5a), which is similar to previous findings [30-35]. At a GO dosage of 0.01 wt. %, hydration products of a rhombohedral symmetry formed, as shown in Fig. 5b-c, which is similar to the morphology of synthetic layered double hydroxides (LDHs) discovered by previous studies [36-37]. LDHs, which often appear as hydrotalcite or other variants in AAS, are well known as one of the main hydration products when magnesium is present [30-33]. This has been investigated using XRD, SEM-EDS and MAS NMR methods on AAS pastes. Furthermore, no obvious crystal structure of LDHs was found in the previous studies [30-31, 33], except using the micro-

8

reactor approach [35], which was carried out using FIB/SEM. When the GO dosage was 0.03 wt. % and

0.05 wt. %, flower-like parallelly grouped crystals were found in hardened AAS pastes. The crystal druse

grew larger (see Fig. 5d-e), mainly due to the greater content of GO nanosheets.

The chemical composition of the crystals in the GO-added AAS pastes was subsequently

determined by SEM-EDS analysis (see Fig. 6). The chemical analysis results show that calcium, silicon,

aluminium and magnesium were the main elements in the rhombohedral symmetry, which is similar to

the hydrotalcite-like LDH products in AAS pastes reported by Mobasher et al [30].

Fig. 7 illustrates the XRD analysis of AAS pastes with various contents of GO after 28 days curing

at 20 °C. A main wide and disperse peak at 29˚ was identified as the main hydration product C-(A)-S-H

gel in the AAS pastes, as was widely reported and verified in recent studies [12, 30-35]. A relatively

lower-intensity peak at approximately 11˚ 2θ was also found in all of the samples, which can be attributed

to the formation of an LDH phase [30-31, 36-37].

In Section 3.2, the decrease in the compressive strength and increase in the flexural strength in GO-

added AAS mortars may be mainly associated with the formation of LDH crystals. An LDH-type phase

could also exist in the plain AAS pastes, but it generally occurs as a near micro-scale combination with

C-S-H gel [30, 39-40]. The addition of GO increases the size of the LDHs and promotes the growth of

crystals. The growth and existence of flake-like crystals could cause defects in the AAS paste matrix and

further decrease the compressive strength. On the other hand, the flake-like crystals could enhance the

bonding between the GO and the matrix and thereby may improve the flexural strength. More

specifically, the GO with an extra high specific area provides a template in the AAS system so that

the C-(A)-S-H gel can grow on the surface of the GO due to the cross-linking between the functional

groups on the GO and the divalent ions in the gel [22]. Hence, significant reinforcement of the AAS

by the GO can be attributed to strong interfacial adhesion between the GO and C-(A)-S-H [41, 42].

3.4 Formation mechanism of LDHs in GO-added AAS pastes

LDHs, which are often synthesised through a chemical approach, have a general formula of $M^{2+}_{1-x}M^{3+}_x(OH)_2A_x \cdot nH_2O$, where M^{2+} stands for Mg^{2+}, Zn^{2+} etc., M^{3+} stands for Al^{3+}, Fe^{3+} and so on, and A_x stands for $1/2(CO_3^{2-})$, Cl^- or OH^- [37]. In alkali-activated slags with a moderate MgO content, the LDHs are identified as $Mg_6Al_2(CO_3)(OH)_{16} \cdot 4H_2O$ [31] or variants. In chemical engineering, the most commonly used method to synthesise LDHs on the surface of GO is to introduce divalent and trivalent cations from solution [43] and then form chemical cross-linking between the cations and the functional groups on the surface of the GO [41]. Due to a co-precipitation process, precipitation will occur, thereby leading to the in situ growth of the LDH phase [38]. Based on previous studies [37, 31], the formation mechanism for LDHs in AAS pastes has been proposed, and a simple sketch is shown in Fig. 8. First, in a condition of alkaline liquor, the slag is dissolved, and Mg^{2+} and Al^{3+} together with other ions such as Ca^{2+} and Na^+ are released to the liquid phase. In GO-added AAS, the negative charge of the GO surfaces leads to a gathering of positive ions including Mg^{2+} and Al^{3+}. In a high alkalinity environment, the Al^{3+} could easily form $Al(OH)_4^-$. With the increasing concentrations of Mg^{2+} and $Al(OH)_4^-$, the continuous reaction between ions generates the obvious LDHs. Therefore, the possible reaction pathways are proposed as follows in GO-added AAS:

In the high pH condition, $Al^{3+} + 4OH^- \rightleftharpoons Al(OH)_4^-$

$$aMg^{2+} + Al(OH)_4^- + (2a-2)OH^- + xH_2O + A^- \rightleftharpoons Mg_aAl(OH)_{2+2a}A \cdot xH_2O(s)$$
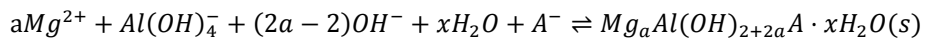
where A^- stands for $1/2\ CO_3^{2-}$ or OH^-.

It is believed that the A^- is more likely verified as OH^- and the possibility of the presence of CO_3^{2-} is mainly due to the absorption of CO_2 from the air.

4. Conclusions

GO nanosheets well-dispersed in an aqueous solution were successfully prepared using the modified Hummers' method. The effects of the GO on the fluidity and microstructure of alkali-activated slag mortars and pastes were investigated. The following conclusions have been drawn based on results obtained:

(1) The fluidity of AAS mortars is significantly reduced with the increasing content of GO.

(2) The introduction of GO into AAS mortars increases the flexural strengths and decreases the compressive strength. The increase rate of the flexural strength can reach 20% after 7 days curing in standard conditions (20 °C, RH $\geq$ 95%). The optimal content of GO is 0.01% by weight of slag.

(3) Layered double hydroxides (LDHs) are formed in GO-added AAS pastes, which are responsible for the changes in mechanical properties. With the increasing dosage of GO, the crystal dimensions become larger, and a flower-like crystal druse is generated. A formation mechanism is proposed based on this and previous studies. The main reaction pathway is regarded as

$$aMg^{2+} + Al(OH)_4^- + (2a-2)OH^- + xH_2O + A^- \rightleftharpoons Mg_aAl(OH)_{2+2a}A \cdot xH_2O(s)$$
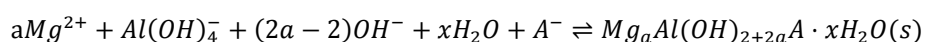
where A^- is most likely OH^- or $1/2\ CO_3^{2-}$.

The results suggest that GO could significantly affect the hydration process, influence the microstructure, and improve the mechanical properties of AAS. This study also suggests a potential application of GO in AAS materials. Further studies on durability, shrinkage behaviours and compatibility with other materials will provide a deeper understanding on this nano-carbon material.

Acknowledgments

Reference

[1] Juenger M C G, Winnefeld F, Provis J L, et al. Advances in alternative cementitious binders[J]. Cement and Concrete Research, 2011, 41(12):1232-1243.

[2] Yang K, Yang C, Magee B, et al. Establishment of a preconditioning regime for air permeability and sorptivity of alkali-activated slag concrete[J]. Cement and Concrete Composites, 2016, 73: 19-28.

[3] Deventer J S J V, Provis J L, Duxson P, et al. Chemical Research and Climate Change as Drivers in the Commercial Adoption of Alkali Activated Materials[J]. Waste and Biomass Valorization, 2010, 1(1):145-155.

[4] Turner L K, Collins F G. Carbon dioxide equivalent (CO2-e) emissions: A comparison between geopolymer and OPC cement concrete[J]. Construction and Building Materials, 2013, 43(6):125-130.

[5] Thomas R J, Ye H, Radlińska A, et al. Alkali-Activated Slag Cement Concrete[J]. Concrete International, 2016, 1: 33-38.

[6] Wang S D, Pu X C, Scrivener K L, et al. Alkali-activated slag cement and concrete: a review of properties and problems[J]. Advances in Cement Research, 1995, 7(27): 93-102.

[7] Bakharev T, Sanjayan J G, Cheng Y B. Resistance of alkali-activated slag concrete to acid attack [J]. Cement and Concrete Research, 2003, 33(10): 1607-1611.

[8] Zhang M, Yang C, Zhao M, et al. Immobilization potential of Cr (VI) in sodium hydroxide activated slag pastes[J]. Journal of Hazardous Materials, 2017, 321:281-289.

[9] Collins F, Sanjayan J G. Cracking tendency of alkali-activated slag concrete subjected to restrained shrinkage[J]. Cement and Concrete Research, 2000, 30(5):791-798.

[10] Collins F, Sanjayan J G. Microcracking and strength development of alkali activated slag concrete[J]. Cement and Concrete Composites, 2001, 23(s 4–5):345-352.

[11] Bernal S, Gutierrez R D, Delvasto S, et al. Performance of an alkali-activated slag concrete reinforced with steel fibers[J]. Construction and Building Materials, 2010, 24(2):208-214.

[12] Rashad A M. A comprehensive overview about the influence of different additives on the properties of alkali-activated slag–A guide for Civil Engineer [J]. Construction and Building Materials, 2013, 47: 29-55.

[13] Chuah S, Pan Z, Sanjayan J G, et al. Nano reinforced cement and concrete composites and new perspective from graphene oxide[J]. Construction and Building Materials, 2014, 73:113-124.

[14] Lv S, Ma Y, Qiu C, et al. Effect of graphene oxide nanosheets of microstructure and mechanical properties of cement composites[J]. Construction and Building Materials, 2013, 49(12):121-127.

[15] Hao W, Ma H, Lu Z, et al. Design of magnesium phosphate cement based composite for high performance bipolar plate of fuel cells[J]. Rsc Advances, 2016, 2016(6):56711-56720.

[16] Lu Z, Hou D, Ma H, et al. Effects of graphene oxide on the properties and microstructures of the magnesium potassium phosphate cement paste[J]. Construction and Building Materials, 2016, 119:107-112.

[17] Zhu Y, Murali S, Cai W, et al. Graphene and Graphene Oxide: Synthesis, Properties, and Applications[J]. Advanced Materials, 2010, 22(35):3906-24.

[18] Pan Z, et al., Graphene oxide reinforced cement and concrete. 2012, WOPatent App. PCT/AU2012/001,582.

[19] Lv S, Liu J, Sun T, et al. Effect of GO nanosheets on shapes of cement hydration crystals and their

formation process[J]. Construction and Building Materials, 2014, 64(64):231-239.

[20] Li X, Korayem A H, Li C, et al. Incorporation of graphene oxide and silica fume into cement paste: A study of dispersion and compressive strength[J]. Construction and Building Materials, 2016, 123:327-335.

[21] Saafi M, Tang L, Fung J, et al. Enhanced properties of graphene/fly ash geopolymeric composite cement[J]. Cement and Concrete Research, 2015, 67(67):292-299.

[22] Park S, Lee K S, Bozoklu G, et al. Graphene oxide papers modified by divalent ions-enhancing mechanical properties via chemical cross-linking.[J]. Acs Nano, 2008, 2(3):572-8.

[23] Huang Q, Wang C, Zeng Q, et al. Deterioration of mortars exposed to sulfate attack under electrical field[J]. Construction and Building Materials, 2016, 117: 121-128.

[24] Stobinski L, Lesiak B, Malolepszy A, et al. Graphene oxide and reduced graphene oxide studied by the XRD, TEM and electron spectroscopy methods[J]. Journal of Electron Spectroscopy and Related Phenomena, 2014, 195(15):145-154.

[25] Galande C, Yalcin S E, Singh A, et al. Photo Induced Fluorescence Enhancement and Correlated FTIR of Single Layer Graphene Oxide[C]// APS March Meeting 2014. American Physical Society, 2014.

[26] You J M, Han H S, Lee H K, et al. Enhanced electrocatalytic activity of oxygen reduction by cobalt-porphyrin functionalized with graphene oxide in an alkaline solution[J]. International Journal of Hydrogen Energy, 2014, 39(10):4803-4811.

[27] Dan L, Müller M B, Scott G, et al. Processable aqueous dispersions of graphene nanosheets.[J]. Nature Nanotechnology, 2008, 3(2):101-5.

[28] Shang Y, Zhang D, Yang C, et al. Effect of graphene oxide on the rheological properties of cement pastes[J]. Construction and Building Materials, 2015, 96:20-28.

[29] Liu J, Li Q, Xu S. Influence of nanoparticles on fluidity and mechanical properties of cement mortar[J]. Construction and Building Materials, 2015, 101:892-901.

[30] Mobasher N, Bernal S A, Provis J L. Structural evolution of an alkali sulfate activated slag cement[J]. Journal of Nuclear Materials, 2015, 468.

[31] Bernal S A, Nicolas R S, Myers R J, et al. MgO content of slag controls phase evolution and structural changes induced by accelerated carbonation in alkali-activated binders[J]. Cement and Concrete Research, 2014, 57(3):33-43.

[32] Fernández-Jiménez A, Puertas F, Sobrados I, et al. Structure of Calcium Silicate Hydrates Formed in Alkaline‐Activated Slag: Influence of the Type of Alkaline Activator[J]. Journal of the American Ceramic Society, 2004, 86(8):1389-1394.

[33] Jin F, Al-Tabbaa A. Strength and drying shrinkage of slag paste activated by sodium carbonate and reactive MgO[J]. Construction and Building Materials, 2015, 81:58-65.

[34] Suraneni P, Palacios M, Flatt R J. New insights into the hydration of slag in alkaline media using a micro-reactor approach[J]. Cement and Concrete Research, 2015, 79.

[35] Ke X, Bernal S A, Provis J L. Controlling the reaction kinetics of sodium carbonate-activated slag cements using calcined layered double hydroxides[J]. Cement and Concrete Research, 2016, 81:24-37.

[36] Hibino T, Ohya H. Synthesis of crystalline layered double hydroxides: Precipitation by using urea hydrolysis and subsequent hydrothermal reactions in aqueous solutions[J]. Applied Clay Science, 2009, 45(3):123-132.

[37] Xu Z P, Lu G Q. Hydrothermal Synthesis of Layered Double Hydroxides (LDHs) from Mixed MgO and Al2O3: LDH Formation Mechanism[J]. Chemistry of Materials, 2005, 17(5):1055-1062.

[38] Cao Y, Li G, Li X. Graphene/layered double hydroxide nanocomposite: Properties, synthesis, and

applications[J]. Chemical Engineering Journal, 2016, 292:207-223.

[39] Richardson I G. The nature of C-S-H in hardened cements[J]. Cement and Concrete Research, 1999, 29(8):1131-1147.

[40] Taylor R, Richardson I G, Brydson R. Composition and microstructure of 20-year-old ordinary Portland cement–ground granulated blast-furnace slag blends containing 0 to 100% slag[J]. Cement and Concrete Research, 2010, 40(40):971-983.

[41] Pan Z, He L, Qiu L, et al. Mechanical properties and microstructure of a graphene oxide–cement composite[J]. Cement & Concrete Composites, 2015, 58:140-147.

[42] Lu Z, Hou D, Meng L, et al. Mechanism of cement paste reinforced by graphene oxide/carbon nanotubes composites with enhanced mechanical properties[J]. Rsc Advances, 2015, 5(5):100598-100605.

[43] He J, Wei M, Li B, et al. Preparation of Layered Double Hydroxides[J]. Interface Science & Technology, 2004, 1(1):345-373.